Eur. Phys. J. E **9**, 301–311 (2002)
DOI 10.1140/epje/i2002-10063-7

THE EUROPEAN PHYSICAL JOURNAL E

Structure of colloidal complexes obtained from neutral/polyelectrolyte copolymers and oppositely charged surfactants

J.-F. Berret[1,a], G. Cristobal[1], P. Hervé[1], J. Oberdisse[2], and I. Grillo[3]

[1] Complex Fluids Laboratory, CNRS - Cranbury Research Center Rhodia Inc., 259 Prospect Plains Road CN 7500, Cranbury NJ 08512, USA
[2] Laboratoire Léon-Brillouin, CEA Saclay, F-91191 Gif-sur-Yvette, France
[3] Institute Laue-Langevin, BP 156, F-38042 Grenoble cedex 9, France

Received 24 July 2002 /
Published online: 21 January 2003 –

Abstract. We report on the phase behavior and scattering properties of colloidal complexes made from block copolymers and surfactants. The copolymer is poly(sodium acrylate)-b-poly(acrylamide), hereafter abbreviated as PANa-PAM, with molecular weight 5000 g/mol for the first block and 30000 g/mol for the second. In aqueous solutions and neutral *p*H, poly(sodium acrylate) is a weak polyelectrolyte, whereas poly(acrylamide) is neutral and in good-solvent conditions. The surfactant is dodecyltrimethylammonium bromide (DTAB) and is of opposite charge with respect to the polyelectrolyte block. Combining dynamical light scattering and small-angle neutron scattering, we show that in aqueous solutions PANa-PAM diblocks and DTAB associate into colloidal complexes. For surfactant-to-polymer charge ratios Z lower than a threshold ($Z_C \sim 0.3$), the complexes are single surfactant micelles decorated by few copolymers. Above the threshold, the colloidal complexes reveal an original core-shell microstructure. We have found that the core of typical radius 100–200 Å is constituted from densely packed surfactant micelles connected by the polyelectrolyte blocks. The outer part of the colloidal complex is a corona and is made from the neutral poly(acrylamide) chains. Typical hydrodynamic sizes for the whole aggregate are around 1000 Å. The aggregation numbers expressed in terms of numbers of micelles and copolymers per complex are determined and found to be comprised between 100–400, depending on the charge ratio Z and on the total concentration. We have also shown that the sizes of the complexes depend on the exact procedure of the sample preparation. We propose that the driving mechanism for the complex formation is similar to that involved in the phase separation of homopolyelectrolyte/surfactant systems. With copolymers, the presence of the neutral blocks prevents the macroscopic phase separation from occurring.

PACS. 82.70.-y Disperse systems; complex fluids – 82.35.Rs Polyelectrolytes – 61.12.-q Neutron diffraction and scattering

1 Introduction

The complexation of polyelectrolytes with oppositely charged species has recently attracted much attention, essentially because of the potential applications in polymer science and biology. Experimentally, polyelectrolyte chains have been studied in aqueous solutions, and so far associated with a broad range of compounds, including oppositely charged polymers (homopolymer, copolymer and dendrimers), colloids (surfactant micelles) and biological macromolecules (proteins, DNA) [1]. On the theoretical side, the electrostatic interactions between oppositely charged macromolecules and colloids of different structures have also been the focus of several studies [2].

The complexes that have been the most extensively investigated during the past years are those made from polymers and surfactants. When homopolyelectrolytes are mixed with oppositely charged surfactants in aqueous solutions, two phenomena are successively observed. First, at very low concentration, the surfactants and polyelectrolyte self-assemble into aggregates comparable to surfactant micelles. Here, however, one or several polyelectrolyte chains can be adsorbed on the micellar surface. This phenomenon occurs at the critical aggregation concentration (cac) which is typically 100–1000 times lower than the regular critical micellar concentration (cmc). The self-assembly mechanism is driven by the binding of polyelectrolyte to the surfactant molecules and by an exchange of the counterions [3,4].

[a] e-mail: jeanfrancois.berret@us.rhodia.com

As the surfactant concentration is further increased, a liquid-solid phase separation is observed. The solid phase appears as a precipitate which contains most of the polyelectrolytes and surfactants [5]. The liquid phase contains essentially solvent molecules and some counterions. In recent years, the structure of the concentrated solid phase has attracted much attention. It has been shown using X-ray scattering [6–15] that the solid precipitates exhibit liquid crystalline order reminiscent of the structures found in surfactant/water concentrated phases [16]. Cubic, hexagonal and lamellar phases have been identified so far, indicating a self-assembly of the surfactants into spheres, cylinders and bilayers, respectively. In these ordered structures, the polyelectrolyte chains are assumed to be adsorbed at the surface of the aggregates, and eventually to link them [9,12,17]. The phase separation has been observed using linear polyelectrolytes, but also using polyelectrolyte cross-linked gels [7,10,11,13].

When the former homopolyelectrolyte chain is one part of a diblock copolymer, the other block being a neutral and water-soluble chain, the phenomena described above are modified. Aqueous solutions of neutral/polyelectrolyte diblocks with surfactants of opposite charge do not exhibit a phase separation. Instead, there is the formation of finite-size colloids made from both surfactant and copolymers. These colloids are also called (surfactant-copolymer) complexes in the literature. Kabanov and co-workers [18–20] have suggested the formation of a core-shell supramolecular assembly where the shell is made from the neutral blocks. Using freeze fracture techniques, these authors found that diblock copolymers and single-tail surfactant arrange spontaneously into vesicles of average size ~ 1000 Å [19]. Very recently, based on a small-angle neutron scattering investigation, we have proposed an alternative picture for the structure of these colloids [21]. We confirm the core-shell structure, but we found that the core is constituted from densely packed surfactant micelles connected between them by polyelectrolyte blocks. The surfactant micelles inside the colloids have nearly the same aggregation number and morphology as if they were dispersed in water above the cmc.

The present paper aims at giving a full account of our investigations on the poly(sodium acrylate)-b-poly(acrylamide) block copolymers with cationic surfactants. Although several molecular weights and weight ratios have been investigated in the course of this study, we are reporting on a single polymer-surfactant system, representative of this class of compounds. The copolymer is characterized by the polyelectrolyte block of molecular weight 5000 g/mol and by the neutral block of molecular weight 30000 g/mol. We have performed dynamic light scattering and small-angle neutron scattering experiments on solutions prepared at low concentrations, that is, below 1% by weight. In the present work, we discuss specifically the effect of the surfactant concentration on the formation of the colloidal complexes. For surfactant-to-polymer charge ratios lower than a threshold, the complexes are single surfactant micelles decorated by one or few copolymers. Above threshold, the colloidal complexes display a core-shell microstructure. The core and the shell are identified from their contributions to the neutron scattering cross-section. A semi-quantitative analysis allows us to determine the respective compositions of the complexes and aggregation numbers.

2 Experimental

2.1 Materials

Poly(sodium acrylate)-b-poly(acrylamide) block copolymers, in short PANa-PAM, were synthesized by controlled radical polymerization in solution. The synthesis is based on the Madix technology which consists in a novel transfer agent-mediated reaction developed by Rhodia [22]. The block copolymer placed under scrutiny has an average molecular weight of 35000 g/mol (polydispersity index 1.6). It is made on average from 70 monomers of acrylic acid ($M_w = 5000$ g/mol) and 420 monomers of acrylamide monomers ($M_w = 30000$ g/mol). In solution, the acrylic acid monomers are ionized by addition of an equivalent amount of sodium hydroxide up to pH 7. At this pH, the ionization of the PAA chains is around 75% [3]. We have also studied the homopolyelectrolyte poly(sodium acrylate) of molecular weight 5000 g/mol for comparison. For both polymers, dodecyltrimethylammonium bromide (DTAB) purchased from Sigma was used as the opposite charged surfactant. Surfactants with longer alkyl chains, such as hexadecyltrimethylammonium bromide were also investigated, and qualitatively, the features of the phase behavior are comparable to those of DTAB. At room temperature, the critical micellar concentration of DTAB is 0.46% [23].

2.2 Phase behavior

Polymer-surfactant phase diagrams were determined experimentally in a concentration range typically below 30%. In the following, the phase diagrams are depicted using for parameters i) the total concentration $\mathbf{c} = \mathbf{c}_P + \mathbf{c}_S$, where $\mathbf{c}_P$ and $\mathbf{c}_S$ are the weight concentrations in polymers and in surfactants, respectively and ii) Z, which is the stoechiometric ratio for chargeable groups. Z is defined as $Z = [S]/(70\times[P])$, where [S] and [P] are the molar concentrations for the surfactant and for the polymer, respectively. $Z = 1$ describes an isoelectric solution, characterized by the same number densities of positive (DTA^+) and negative (COO^-) chargeable ions. Mixed surfactant-polymer solutions at concentration $\mathbf{c}$ and charge ratio Z were prepared by mixing pure surfactant (at $\mathbf{c}$ and $Z = \infty$) and pure polymer (at $\mathbf{c}$ and $Z = 0$) solutions in the right amount. Z is then proportional to the mass ratio of the two liquids. We use the same procedure for the homopolyelectrolytes and for neutral/polyelectrolyte block copolymers. The $(\mathbf{c}, Z)$-phase diagram obtained for the system PANa/DTAB/water is displayed in Figure 1. For total concentration $\mathbf{c}$ between 0.1% and 20%, there exists a value of the stoechiometric

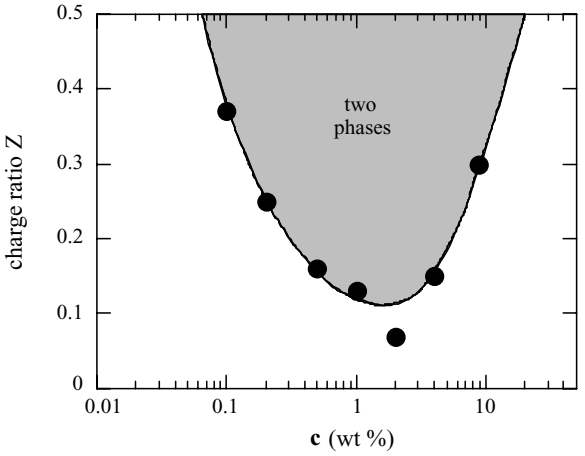

Fig. 1. Phase diagram obtained for the system poly(sodium acrylate) (PANa, M_w = 5000 g/mol), dodecyltrimethylammonium bromide (DTAB) and water. The phase diagram is displayed using **c** and Z for coordinates, where **c** is the total concentration in polymer and in surfactant and Z the stoechiometric ratio for chargeable groups. The shaded area indicates the two-phase region.

ratio above which two phases coexist [9,12,17]. The data points in Figure 1 were obtained from light scattering experiments by measuring the 90° scattering intensity, and by direct visualisation. Above Z_C, the solutions become turbid and after some time, they display two well-separated phases. As explained in reference [9], because the system under scrutiny is a four-components system (polyelectrolyte, simple salt, surfactant and complex salt), the full description of the phase diagram with tie lines and lever rules is more complex than the one displayed in Figure 1. A three-dimensional representation is required instead, which has the form of a pyramid phase diagram with the water at the top and the four components at each corner of a quadratic base. We have confirmed the structure of the PANa/DTAB precipitates by X-ray scattering. We have found clear evidences of a crystalline structure with cubic symmetry (space group $Pm3n$). When the homopolyelectrolyte is replaced by a 5k-30k PANa-PAM diblock copolymer, no phase separation is observed in the ranges of concentrations and charge ratios of Figure 1. The solutions appear homogeneous and transparent.

2.3 Light scattering

Static and dynamic light scattering were performed on a Brookhaven spectrometer (BI-9000AT autocorrelator) for the measurements of the Rayleigh ratio $R_\theta(q, \mathbf{c})$ and of the diffusion constant $D(\mathbf{c})$. The Rayleigh ratio was determined from the scattering intensity at wave vector $q = 2.3 \times 10^{-3}$ Å^{-1} ($\theta = 90°$) normalized with respect to that of toluene. From the extrapolation of $D(\mathbf{c})$ to infinite dilution, the hydrodynamic radius of the colloids was calculated through the Stokes-Einstein relation, $R_H = k_B T/6\pi\eta_0 D(\mathbf{c} \to 0)$, where k_B is the Boltzmann constant, T the temperature (T = 298 K) and η_0 the solvent viscosity.

Table 1. Coherent scattering lengths (b in 10^{-12} cm), molecular volumes (V in Å^3) and coherent scattering length densities (ρ in 10^{10} cm^{-2}) of the chemical species studied in this work.

Species	b (10^{-12} cm)	V (Å^3)	$\rho(10^{10}\,\mathrm{cm}^{-2})$
DTAB	−1.14	486	−0.23
DTA^+	−1.82	447	−0.41
CH_2-CHCOOH	+1.66	114	+1.46
CH_2-$CHCOO^-$,Na^+	+2.40	149	+1.61
CH_2-$CHCONH_2$	+1.64	105	+1.56
D_2O	+1.915	30	+6.38

2.4 Small-angle neutron scattering

Small-angle neutron scattering (SANS) was performed at three different neutron facilities, at Argonne (USA), at the Laboratoire Léon Brillouin (Saclay, France) and at the Institute Laue-Langevin (Grenoble, France). All runs were consistent with each other. Here, only the data obtained on the D22 beam line of the Institute Laue-Langevin are shown and discussed. Solutions at concentrations **c** = 0.25%–20% and surfactant-to-monomer ratios $Z = 0$–∞ were prepared using D_2O for contrast reasons. In the present report, we focus on dilute solutions, typically below **c** = 1%, because we aimed at determining the form factor of the colloidal complexes. The coherent neutron scattering lengths for acrylamide, for sodium acrylate and for DTAB are 1.56, 1.61 and $-0.25 \times 10^{10}\,\mathrm{cm}^{-2}$, respectively. Thus, in D_2O (density $\rho_0 = 6.38 \times 10^{10}\,\mathrm{cm}^{-2}$) all three components are contributing to the total cross-section. The list of the coherent scattering lengths, molecular volumes and coherent scattering length densities of the chemical species studied in this work are given in Table 1. On D22, the data collected at 2 m and 14 m cover a range in wave vector: 1.5×10^{-3} Å^{-1} and 0.25 Å^{-1}, with an incident wavelength of 12 Å. They are treated according to the standard procedures.

3 Results

3.1 Light scattering

For light scattering experiments, PANa-PAM/DTAB solutions were prepared in H_2O at total concentrations **c** = 0.1% and **c** = 1% with Z comprised between 0.01 and 1000. The Rayleigh ratios measured at $q = 2.3 \times 10^{-3}$ Å^{-1} for these two series are shown in Figure 2. At low values of Z, typically below 0.4, the scattering intensity is independent of the surfactant concentration and it remains at the level of the pure polymer (Z = 0). Above a critical Z, noted Z_C, the Rayleigh ratio increases by several orders of magnitude, indicating the formation of large aggregates. Dynamical light scattering for solutions above

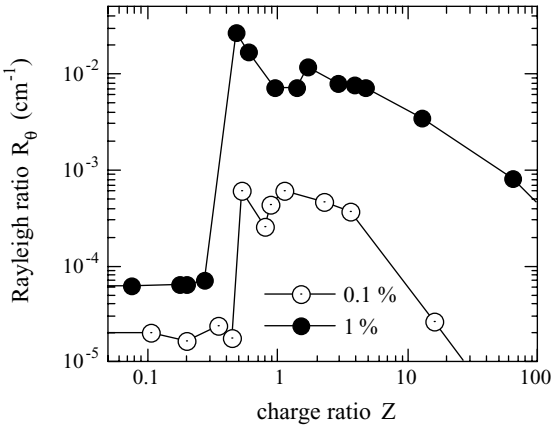

Fig. 2. Rayleigh ratios measured for aqueous solutions of charged/neutral copolymer (PANa-PAM) and oppositely charged surfactant (DTAB) at $\mathbf{c} = 0.1\%$ and $\mathbf{c} = 1\%$, as a function of the charge ratio Z. The experiments are performed at ambient temperature and scattering angle $\theta = 90°$ ($q = 2.3 \times 10^{-3}$ Å^{-1}). Above the critical value $Z_C \sim 0.4$, the Rayleigh ratio increases by several orders of magnitude.

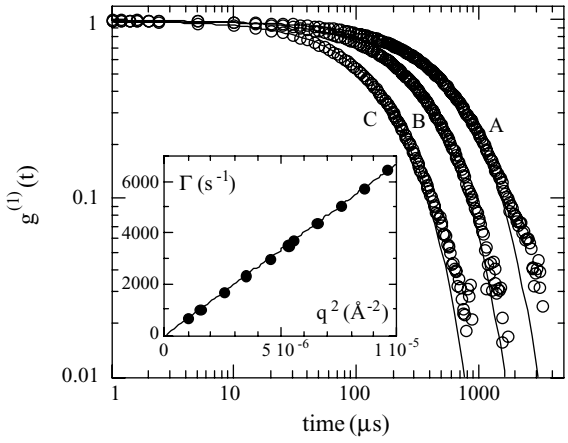

Fig. 3. First-order normalized autocorrelation function $g^{(1)}(t)$ of the intensity scattered by PANa-PAM/DTAB aqueous solutions at $\mathbf{c} = 0.1\%$ and $Z = 1$. The data correspond to scattering wave vectors $q = 1.6$ (A), 2.1 (B) and 3.0×10^{-3} Å^{-1} (C). Continuous lines are single exponential functions with decay rate Γ. Inset: evidence of the quadratic dependence of Γ *versus* wave vector. The slope, $D(\mathbf{c} \to 0) = 6.7 \times 10^{-12}\,\mathrm{m^2 s^{-1}}$ corresponds to a hydrodynamic radius $R_H = 370$ Å.

Z_C shows a remarkable behavior illustrated in Figure 3. Here, the first-order normalized autocorrelation function of the scattered intensity $g^{(1)}(t)$ is shown as a function of the delay time for different wave vectors. The relaxation functions labeled A, B and C were recorded at $q = 1.6$, 2.1 and 3.0×10^{-3} Å^{-1}, respectively. Continuous lines through the data points are best-fit calculations using a single exponential function of decay rate Γ. In the inset of Figure 3, the linear dependence of $\Gamma(q)$ *versus* q^2 evidences the diffusive character of the concentration fluctuations. The diffusion coefficient $D(\mathbf{c} \to 0) = 6.7 \times 10^{-12}\,\mathrm{m^2 s^{-1}}$ corresponds to an hydrodynamic radius $R_H = 370 \pm 10$ Å.

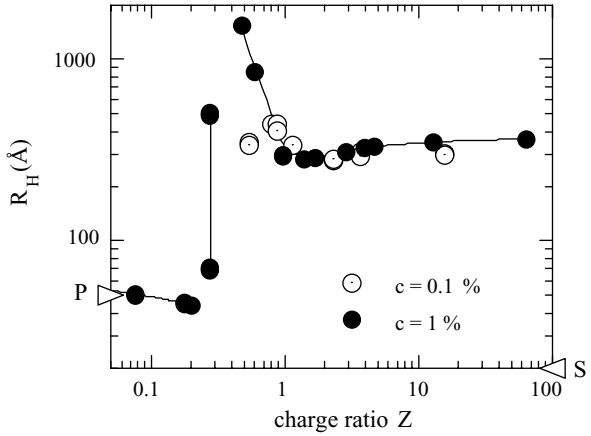

Fig. 4. Z-dependence of the hydrodynamic radius R_H for PANa-PAM/DTAB solutions at $\mathbf{c} = 0.1\%$ and 1%. With increasing Z, R_H passes from sizes consistent with that of single diblock molecules (indicated by a triangle and by the letter P) to much larger values above Z_C, $R_H \sim 350$ Å. In the transition range, we observe a coexistence of these two diffusion modes. The radius of the surfactant micelles is also shown by a triangle on the right side of the plot, and by the letter S.

The analysis of the autocorrelation functions in terms of cumulants reveals a relatively narrow polydispersity of the particle sizes. Figure 4 displays the evolution of the hydrodynamic radius on the whole range of charge ratios. At $\mathbf{c} = 0.1\%$, measurements could not be performed below $Z_C \sim 0.6$, due to a very weak scattering signal. Above Z_C, we observe a hydrodynamic radius rather constant in Z around 350 Å. At $\mathbf{c} = 1\%$, three scattering regimes can be distinguished. At low Z, R_H is 40–50 Å, a value consistent with the hydrodynamic radius of a single diblock molecule [24]. Close to $Z_C = 0.25$, the first-order autocorrelation function $g^{(1)}(t)$ reveals the coexistence of two diffusive modes: a fast mode associated to the diffusion of single diblock molecules, and one slow mode related to the diffusion of colloids of larger sizes. In Figure 4, between Z_C and 1, R_H passes through a maximum at around 1500 Å, and then decreases to R_H-values in accordance with those obtained at $\mathbf{c} = 0.1\%$.

3.2 Small-angle neutron scattering

Figures 5a and 5b show the scattering intensity obtained for PANa-PAM/DTAB solutions in D_2O at $\mathbf{c} = 1\%$, for different values of Z, between $Z = 0$ (pure polymer) and $Z = \infty$ (pure surfactant). For the sake of clarity, all data sets are shifted with respect to each other by a multiplicative factor given in the caption. The pure polymer solution exhibits an overall weak scattering (Fig. 5a), as is expected from dilute polymer solutions in good-solvent conditions. The scattering intensity from the pure surfactant solution is also modest (Fig. 5b); however, it exhibits a broad correlation bump around 0.05 Å^{-1} attributed to electrostatic interactions between DTAB micelles [25]. For the mixed PANa-PAM/DTAB solutions, there exists a critical stoechiometric ratio (here $Z_C \sim 0.3$) above which

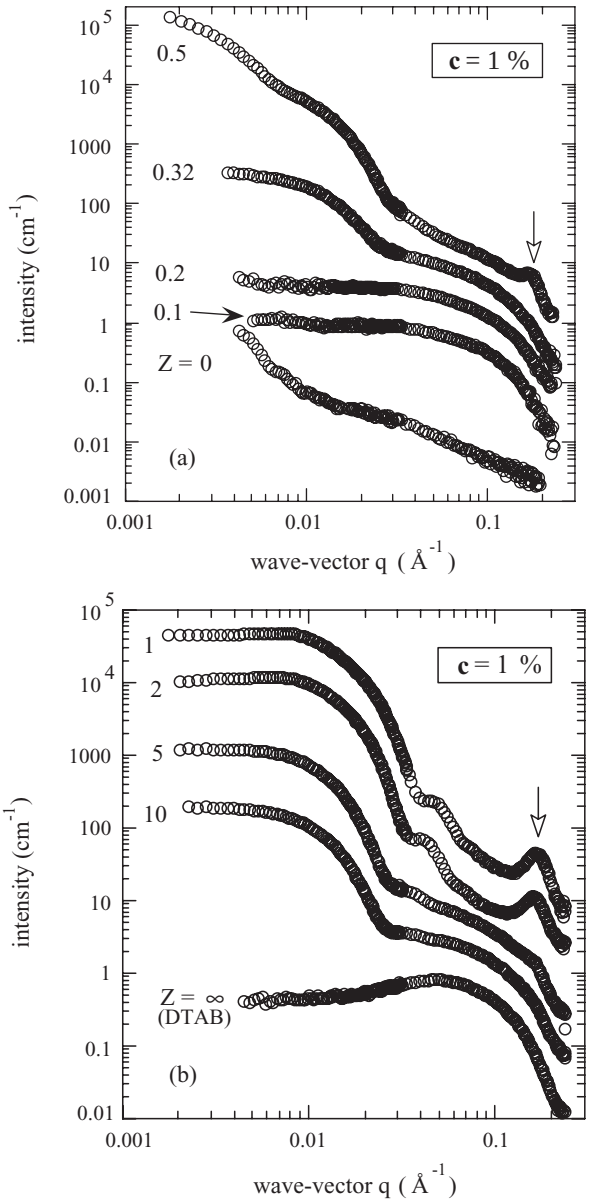

Fig. 5. Neutron scattering intensities obtained for PANa-PAM/DTAB aqueous solutions at $\mathbf{c} = 1\%$ and Z varying from 0 to 0.5 (a) and from 1 to ∞ (b). In (a), the data have been shifted by the multiplicative factor 10 ($Z = 0.1$), 20 ($Z = 0.2$), 50 ($Z = 0.32$) and 200 ($Z = 0.5$) with respect to the data at $Z = 0$ (pure copolymer). In (b), these coefficients are 5 ($Z = 10$), 20 ($Z = 5$), 200 ($Z = 2$) and 1000 ($Z = 1$) and the reference curve is $Z = \infty$ (pure surfactant). An arrow indicates the position of a structure peak at $q_0 \sim 0.16$ Å^{-1}.

the scattering intensity is dominated by the two noticeable features: a strong forward scattering ($q \to 0$) and the appearance of a structure peak at high wave vectors. This peak is located at $q_0 \sim 0.16$ Å^{-1} and shown by an arrow (Figs. 5). It should be emphasized that for PANa-PAM/DTAB, as well as for the different systems investigated during the course of this work (changing the nature or molecular weight of the polyelectrolyte, or changing the surfactant hydrophobicity), these two features have been

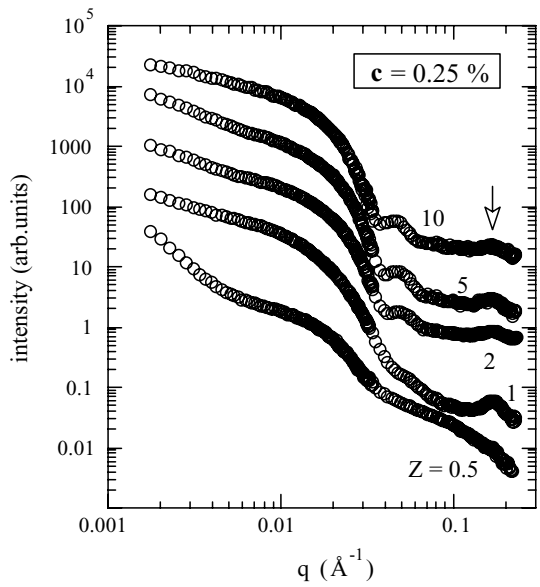

Fig. 6. Same as in Figure 5, but for total concentration $\mathbf{c} = 0.25\%$.

always and systematically found to be correlated. Note in Figure 5b for $Z = 1$ and $Z = 2$ the damped oscillation in the intensity decay around 0.05 Å^{-1}.

PANa-PAM/DTAB solutions prepared in D_2O at $\mathbf{c} = 0.25\%$ present typically the same characteristics than the ones previously described for $\mathbf{c} = 1\%$. In Figure 6, the scattering functions are also shifted with respect to each other for the sake of clarity. The essential difference with the data at $\mathbf{c} = 1\%$ is indeed visible at low wave vectors. Below 0.01 Å^{-1}, the scattering continues to grow with decreasing q, whereas at $\mathbf{c} = 1\%$ the intensity levels off, presenting eventually a slight maximum (as for $Z = 1$ and 2 around 0.006 Å^{-1}, Fig. 5b). The data obtained at $\mathbf{c} = 0.25\%$ can be regarded as the form factors of the aggregates. In the rest of the paper, we use the term *colloidal complexes* to designate these aggregates.

4 Analysis and discussion

4.1 Evidences of decorated surfactant micelles ($Z < Z_C$)

In this section, we analyze the neutron scattering behaviors shown by PANa-PAM/DTAB solutions at low surfactant concentrations. Three spectra in Figure 5a have been selected to this aim, the ones at $Z = 0.1$, 0.2 and $Z = 0.32$. The neutron scattering data for these three solutions are plotted in Figure 7 using a Guinier representation for spherical particles: the intensity is displayed in a semi-logarithmic scale as a function of the square of the wave vector. Only data at large wave vectors are considered. In Figure 7, all three solutions exhibit an exponential decrease of the intensity *versus* q^2. The straight lines result from best-fit calculations using the expression

$$I\ (c, Z, q)\ = I\ (c, Z, q \to 0) \times \exp\left(-\frac{q^2\, R_G^2}{3}\right), \qquad (1)$$

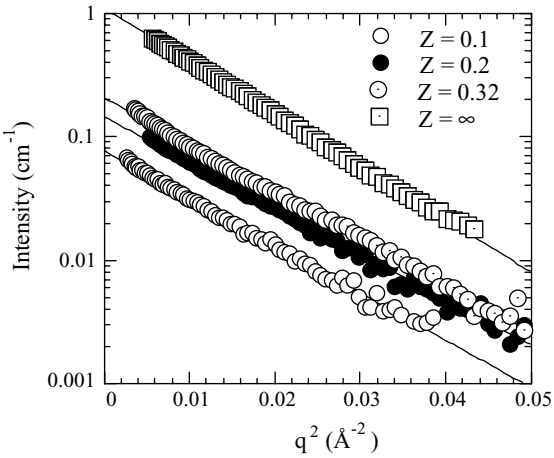

Fig. 7. Guinier representation ($\log I(q)$ *versus* q^2) of the neutron scattering data obtained from PANa-PAM/DTAB solutions at $Z = 0.1$, 0.2 and $Z = 0.32$ and $\mathbf{c} = 1\%$. Data for pure DTAB are shown for comparison. From the slope of the linear decrease (Eq. (1)), we get radii of gyration $R_G = 16.0 \pm 0.3$ Å. The result suggests that although the surfactant concentration is below the cmc (see Tab. 2), DTA micelles are formed and decorated by diblock copolymers.

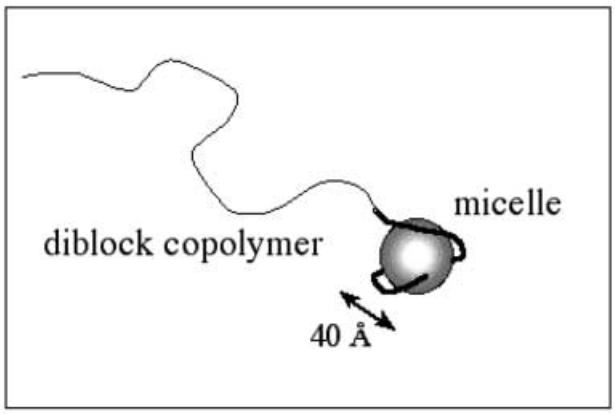

Fig. 8. Schematical representation of DTA micelles decorated by one PANa-PAM block copolymer. This picture is deduced from the neutron scattering results at low surfactant-polymer ratios (Fig. 7, $Z < Z_C$).

where $I(c, Z, q \to 0)$ is the intensity extrapolated at zero wave vector and R_G the radius of gyration of the particles. These two quantities are adjustable parameters in the fitting. For $Z = 0.1$–0.32, one finds a radius of gyration $R_G = 16.0 \pm 0.3$ Å, which corresponds to an actual radius of 20.6 ± 5 Å (assuming homogeneous particles). The data obtained on the DTAB micellar solution at $\mathbf{c} = 1\%$ ($Z = \infty$) are included in Figure 7 for comparison. The slope of the intensity decrease is very close to those found for $Z = 0.1$–0.32 and consistent with a radius $R_G = 17$ Å. These results suggest that the particles detected by neutron scattering are spherical micelles. In the following, for the mixed polymer-surfactant systems for which it can be assumed that most of the bromide counterions have been replaced by polyacrylate, the expression "DTA micelles" will be preferred to that of "DTAB micelles". In Table 2, we have listed the parameters received from the Guinier analysis, as well as the aggregation number N^S_{Agg} (number of surfactants molecules per micelle) derived using a simple geometrical model. We obtain $N^S_{Agg} \sim 70$.

A second result of Figure 7 confirms this finding. The prefactor in equation (1), $I(c, Z, q \to 0)$ is found to be proportional to Z, *i.e.* it is proportional to the surfactant concentration. It can be assumed then, that for the three samples considered, all surfactant molecules are associated into spherical micelles of radius R_{Mic} of about 20 Å. $I(c, Z, q \to 0)$ can be written:

$$I\ (c, Z, q \to 0) = \frac{\mathbf{c}_S\, \mathcal{N}_A}{M^S_w\, N^S_{Agg}} \left(V_{Mic}\, \Delta\rho_S\right)^2 , \qquad (2)$$

where $\mathcal{N}_A$ is the Avogadro number, M^S_w is the molecular weight of a surfactant ($M^S_w = 308$ g/mol), V_{Mic} the volume of the particle and $\Delta\rho_S = \rho_S - \rho_0 = 6.6 \times 10^{10}$ cm^{-2} the scattering length contrast between surfactant and solvent. The aggregation numbers determined from equation (2) are around $N^S_{Agg} = 80$, with a relative uncertainty of 10% (Tab. 2). These results are in good agreement with the values deduced from the radii of gyration, and also in good agreement with those known from the literature [23].

The argument that leads us to conclude that the DTA micelles at $Z = 0.1$–0.32 are decorated by copolymers is based on an analogy with homopolyelectrolyte/surfactant systems [1–4]. For the three samples, the surfactant concentration $\mathbf{c}_S$ is below the cmc of DTAB. $\mathbf{c}_S$ ranges from 6×10^{-4} ($Z = 0.1$) to 1.7×10^{-2} ($Z = 0.32$), which is 10 to 3 times lower than the cmc of DTAB (0.46% at ambient temperature). Since the neutron scattering experiments have clearly identified spherical DTA micelles below the cmc, we can conclude that the solutions are above the critical aggregation concentration (cac). By analogy with what is known from the interactions between homopolyelectrolytes and oppositely charged surfactants [4], we also suggest that the polyelectrolyte blocks of PANa-PAM copolymers are adsorbed onto the micellar surfaces. The micelles are dressed or decorated by one or several diblocks. Light and neutron scattering experiments cannot tell, however, the average number of block copolymers adsorbed per micelles. Simple arguments based on the charge balance between micelles and the 70-monomers polyelectrolyte block yield a number of 1 to 3 diblocks per micelle. We propose in Figure 8 a schematical drawing of a DTA micelle decorated by one PANa-PAM block copolymer. It is interesting to note, finally, that the decorated micelles cannot be detected easily by dynamic light scattering experiments (Fig. 4). This is because at low Z there are very few of them. Moreover, their hydrodynamic radius is comparable to that of unassociated diblocks. On the other hand, decorated micelles can be better detected by SANS because of their increased scattering contrast as compared to that of the polymers. In these experiments, we also took advantage of the high flux of the D22 beam line at the Institute Laue-Langevin.

Table 2. List of parameters received from the Guinier analysis of the neutron scattering data at low surfactant concentrations (Fig. 7). In the estimates of the aggregation numbers for decorated micelles, we consider a model where acrylate monomers are adsorbed on the micelles. For simplicity, we assume, as in Figure 8, that there is one adsorbed diblock per micelle. The aggregation number can then be expressed as $N_{\rm Agg}^{\rm S} = 4\pi R_{\rm Mic}^3/3V$, where $V = 447$ Å^3 (for DTA$^+$ molecules) + 112 Å^3 (for acrylate monomer). Similarly, the scattering contrast in equation (2) takes into account the acrylate monomers adsorbed on the surface, yielding $\Delta\rho_{\rm S} = 6.4 \times 10^{10}\,{\rm cm}^{-2}$.

PANa-PAM/DTAB	$\mathbf{c}_{\rm S}$	$I(c, q \to 0)$ ($\rm cm^{-1}$)	$R_{\rm G}$ (Å)	$R_{\rm Mic}$ (Å)	$N_{\rm Agg}^{\rm S}$ from $R_{\rm G}$	$N_{\rm Agg}^{\rm S}$ from $I(c, q \to 0)$
$Z = 0.1$	6.0×10^{-4}	0.088	16.3	21.0	69 ± 5	81 ± 8
$Z = 0.2$	1.2×10^{-3}	0.150	16.0	20.6	65 ± 5	86 ± 8
$Z = 0.32$	1.7×10^{-3}	0.205	16.2	20.9	68 ± 5	97 ± 10
$Z = \infty$	1.0×10^{-2}	1.10	17.0	20.7[a]	76 ± 8	62 ± 6[b]

([a]) In the last column, the aggregation number for DTA micelles at $\mathbf{c}_{\rm S} = 1\%$ is calculated according to equation (2) in which $\mathbf{c}_{\rm S}$ is replaced by $\mathbf{c}_{\rm S} - {\rm cmc}$ (${\rm cmc}_{\rm DTAB} = 0.46\%$ [23]).
([b]) In the last line, the micellar radius $R_{\rm Mic}$ is obtained using a fitting that accounts for the polydispersity [21].

4.2 Structure of the surfactant-polymer complexes ($Z > Z_C$)

4.2.1 Neutron scattering at intermediate wave vectors ($0.01\text{Å}^{-1} < q < 0.1\text{Å}^{-1}$)

Here, we analyze the neutron scattering data of Figures 5 in the range $Z > Z_{\rm C}$, that is, where the intensities exhibit a strong forward scattering and a damped oscillation around 0.05 Å^{-1}. The data for the PANa-PAM/DTAB system at $\mathbf{c} = 1\%$ and $Z = 0.5$, 1, 2 and 5 are displayed in Figure 9 using a Porod representation ($q^4 \times I(q)$ *versus* q). The Porod representation aims at emphasizing the local curvature of interfaces separating the elementary scatterers and solvent molecules. All four samples show damped oscillations which are fitted assuming a distribution of spherical and homogeneous particles, with an average radius $R_{\rm C}$ and a standard deviation $\sigma(R_{\rm C})$. The agreement between the data and the calculated curves is good and for the samples at $Z = 1$ and $Z = 2$, it is excellent. The values for $R_{\rm C}$ and $\sigma(R_{\rm C})$ are given in Table 3 for Z comprised between 0.5 and 10. $R_{\rm C}$ varies typically between 120 Å and 170 Å, with a standard deviation of about 20 Å. The $R_{\rm C}$-values are thus falling in a range which is intermediate between the micellar radius ($R_{\rm Mic} \sim 20$ Å) and the hydrodynamic radius ($R_{\rm H} \sim 400$ Å). Figure 10 illustrates this result. Here, we have plotted for comparison the evolution of $R_{\rm C}$ and $R_{\rm H}$ as a function of Z for PANa-PAM/DTAB solutions at $\mathbf{c} = 1\%$. We have checked that the change of solvent between the solutions prepared for neutron scattering and those prepared for light scattering does not affect the values of the hydrodynamic radius. In Figure 10, we observe a systematic shift of $R_{\rm H}$ with respect to $R_{\rm C}$, $R_{\rm H}$ being typically 3 times larger. This result can be understood if one assumes a core-shell microstructure for the surfactant-copolymer complexes. The core dominates the neutron scattering cross-section at intermediate wave vectors (0.01 Å$^{-1} < q < 0.1$ Å^{-1}), whereas the corona which is made from the neutral poly(acrylamide) blocks is associated with the hydrodynamic size of the colloidal complex.

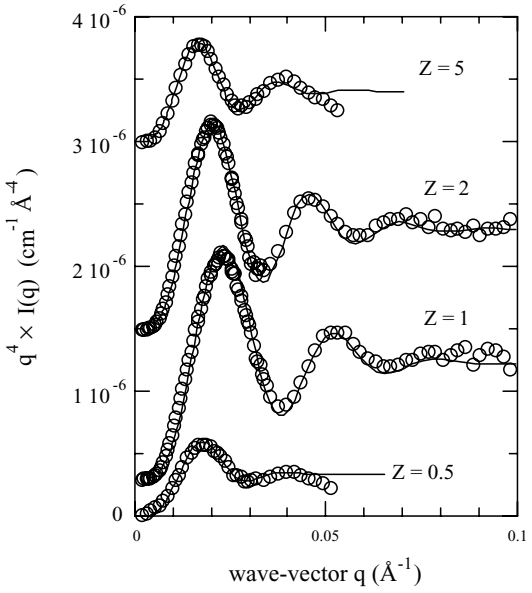

Fig. 9. Porod representation ($q^4 \times I(q)$ *versus* q) of the neutron scattering intensity for PANa-PAM/DTAB solutions at $\mathbf{c} = 1\%$ and $Z = 0.5$, 1, 2 and 5. The damped oscillations are well accounted for by a distribution of spherical and homogeneous particles with an average radius $R_{\rm C}$ and a standard deviation $\sigma(R_{\rm C})$. $R_{\rm C}$-values vary between 120 Å and 180 Å and depend on Z (Tab. 3).

In Figure 10, we observe an increase of the hydrodynamic and core radii in the vicinity of the threshold (with $Z > Z_{\rm C}$). Even very close to $Z_{\rm C}$, there is the evidence of a bimodal distribution of particles. This state of coexistence has been found using both dynamical light scattering (see Fig. 4) and small-angle neutron scattering experiments. In neutron, this finding can be guessed from the data shown in Figure 5a for PANa-PAM/DTAB at $Z = 0.5$. The low-q region of the scattering intensity exhibits two successive Guinier regimes in agreement with the predictions of equation (1) (one for $q < 6 \times 10^{-3}$ Å^{-1} with $R_{\rm G} = 500$ Å and the second for 8×10^{-3} Å$^{-1} < q < 3 \times 10^{-2}$ Å^{-1} with

Table 3. List of the parameters used in the fitting of the neutron scattering data at $\mathbf{c} = 1\%$. We consider here a distribution of spherical particles of radius R_C and standard deviation $\sigma(R_C)$. The average number of micelles per aggregate N_{Agg}^{Mic} is calculated using equation (2). The intensity extrapolated to zero wave vector $I_C(c, Z, q \to 0)$ in equation (3) is used to estimate the number of polymers per colloidal complex.

PANa-PAM/DTAB	R_C (Å)	σ (R_C) (Å)	$I_C(c, Z, q \to 0)$ (cm^{-1})	N_{Agg}^{Mic}
Z = 0.5	165 ± 5	24	40 ± 2	280 ± 30
Z = 0.7	119 ± 4	18	29 ± 2	105 ± 10
Z = 1	124 ± 2	15	40 ± 2	120 ± 5
Z = 2	140 ± 2	16	58 ± 3	170 ± 10
Z = 5	175 ± 4	24	66 ± 4	330 ± 30
Z = 10	178 ± 3	22	38 ± 2	350 ± 20

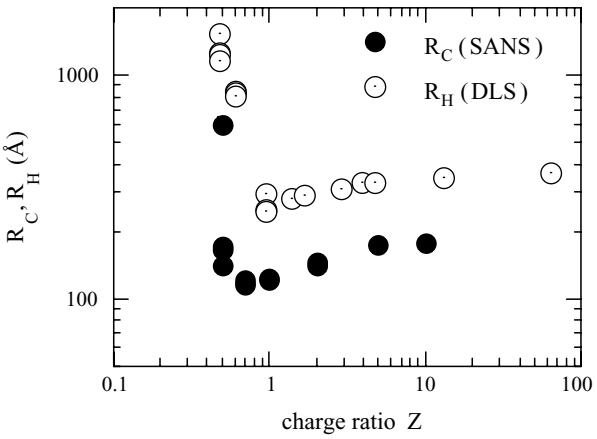

Fig. 10. Evolution of the core and hydrodynamic radii as a function of Z for PANa-PAM/DTAB solutions at $\mathbf{c} = 1\%$. R_C is determined by neutron scattering and R_H by dynamic light scattering. For $Z > Z_C$, R_H is typically 3 times larger than R_C. This result is interpreted as the evidence of a core-shell microstructure for the surfactant-copolymer complexes.

$R_G = 130$ Å). The associated radii are shown in Figure 10. Clearly, the part of the phase diagram comprised between $Z = Z_C$ and $Z = 1$ is more complicated than the simple description we have previously proposed for $Z > 1$. We have no explanation for the bimodal state, nor on the local microstructure of the very large aggregates. This issue will be addressed in a forthcoming publication. We have finally listed in Table 3 the intensity extrapolated to zero wave vector $I_C(c, Z, q \to 0)$ obtained from the Porod fits of Figure 9. If this intensity is assumed to arise solely from the core, $I_C(c, Z, q \to 0)$ can be expressed as

$$I_C(c, Z, q \to 0) = n(Z)\, \overline{\Delta\rho_C}^2\, V_C^2(Z)\,. \qquad (3)$$

In equation (3), $n(Z)$ is the number density of cores (or, equivalently, the number density of colloids) per unit volume, $\overline{\Delta\rho_C}$ is the average scattering contrast of the core with respect to D_2O and $V_C(Z) = 4/3\pi R_C^3$. The above expression will be used to derive the aggregation numbers of surfactant and block copolymers per colloid.

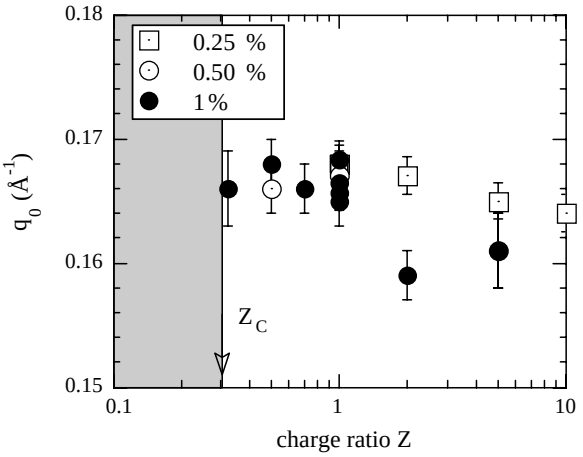

Fig. 11. Position of the structure peak observed at large wave vectors as a function of the stoechiometric ratio Z for PANa-PAM/DTAB solutions $\mathbf{c} = 0.25\%$, $\mathbf{c} = 0.50\%$ and $\mathbf{c} = 1\%$. The mean value $q_0 = 0.165 \pm 0.005$ Å^{-1} corresponds to an average distance $2\pi/q_0 \sim 40$ Å.

4.2.2 Neutron scattering at large wave vectors ($q > 0.1$ Å^{-1})

At large wave vectors and charge ratios above the threshold ($Z > Z_C$), the scattering is characterized by a structure peak at a wave vector noted q_0 (~ 0.16 Å^{-1}). Corresponding to a characteristic distance of 40 Å, this peak is independent of the concentration $\mathbf{c}$, as well as of the surfactant-to-polymer ratio Z. This result is illustrated in Figure 11, where q_0 is shown as a function of Z for three different concentrations, $\mathbf{c} = 0.25\%$, $\mathbf{c} = 0.50\%$ and $\mathbf{c} = 1\%$. In Figure 11, it can be noticed that the first data point is for a PANa-PAM/DTAB solution at $\mathbf{c} = 1\%$ and $Z = 0.32$. However, from the scattering data of Figure 5a no structure peak can be directly observed in the range 0.1–0.2 Å^{-1} for this sample. In order to reveal the presence of a structure peak around q_0, we had to subtract from the raw scattering the Guinier contribution of the DTA micelles (Eq. (1)). Doing so, we end up with a weak intensity which now convincingly exhibits a peak at 0.166 ± 0.004 Å^{-1}. The neutron intensity at $Z = 0.32$ is shown in Figure 12, together with the result of the subtraction described previously (inset). This findings are crucial since they demonstrate that the neutron features characterizing the complexes, namely a strong forward scattering and the structure peak at q_0 are intimately correlated. It has been checked finally with small-angle X-ray scattering that the structure peak is actually broad and does not result from the superposition of several Bragg reflections. A similar structure peak observed in the same q-range and using neutron scattering has been reported recently by Claesson *et al.* on a slightly different system [26].

As for the origin structure peak at q_0, we have two independent indications that it is related to the surfactants. First, its position is found to shift to lower wave

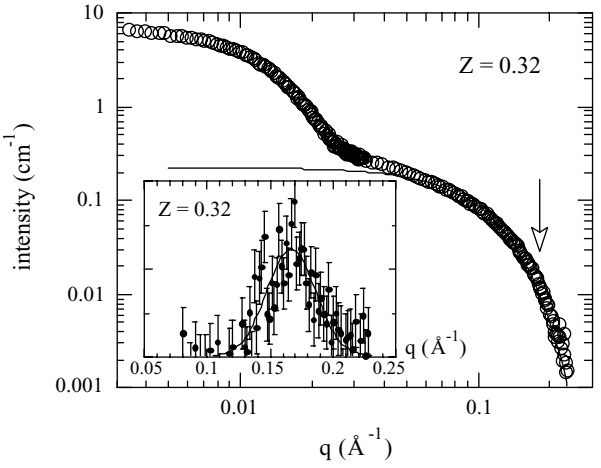

Fig. 12. Neutron scattering intensity *versus* wave vector for a PANa-PAM/DTAB solution at $\mathbf{c} = 1\%$ and $Z = 0.32$. The continuous line is calculated using equation (1) and accounts for the form factor of DTA micelles. In the inset, the result of the subtraction between the experimental data and the calculated Guinier behavior exhibits a very weak structure peak at wave vector $q_0 = 0.166 \pm 0.004$ Å^{-1}.

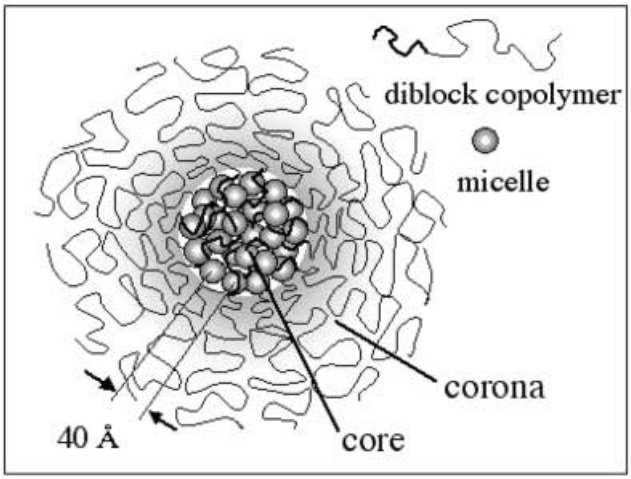

Fig. 13. Schematical representation of a colloid complex formed by the association of polyelectrolyte/neutral diblocks and oppositely charged surfactants, as deduced from light and neutron scattering measurements.

vectors when the length of the amphiphile molecule is increased from 12 (as in DTAB) to 16 carbon atoms (as in cetyltrimethylammonium bromide). Second, when the aliphatic chain of the surfactant is deuterated, the peak vanishes almost completely, indicating a noticeable change in the scattering contrast [26]. We conclude from these observations that the structure peak at $q_0 = 0.165 \pm 0.005$ Å^{-1} arises from a concentrated phase of strongly interacting DTA micelles. One way to reconciliate this result with the fact that the overall concentration of these solutions is low (less than 1%) is to assume that the DTA spherical micelles are located in the core of the colloidal complexes. In this case, we use again the analogy with the homopolyelectrolyte/surfactant concentrated phases [9,12,17] and suggest that the micelles are linked together by the acrylate chains in a relatively dense state. The characteristic distance of $2\pi/q_0 \sim 40$ Å is the intermicellar distance. In terms of symmetry, the core of the colloids can be considered as disordered. In Figure 13, we propose a schematical representation for the colloidal complexes.

4.2.3 Aggregation numbers

Can we evaluate the aggregation numbers of micelles, noted $N_{\mathrm{Agg}}^{\mathrm{Mic}}$, and the number of diblocks copolymers, noted $N_{\mathrm{Agg}}^{\mathrm{P}}$, per colloid? The answer is yes, but some assumptions have to be made. The first assumption is about the relative proportions of the different components forming the core. Since the position of the structure factor at q_0 remains unchanged under both variations of Z or $\mathbf{c}$, the composition of the core can be also considered as constant in terms of surfactants, polyelectrolyte blocks and solvent molecules. However, as shown in Table 3, the radius of the core and the aggregation numbers are still depending on Z. In this reasoning, we do not consider the case of neutral poly(acrylamide) blocks, or part of them being located in the core.

In our first report [21], we used the position of the structure peak at $q_0 \sim 0.16$ Å^{-1} to derive the volume fraction of surfactants in the core. The value of q_0 was compared to the position of the structure factor of pure DTAB solutions. For DTAB in D_2O, small-angle neutron scattering runs were carried out and the scaling law between the maximum of the structure factor and the surfactant concentration was found: $q_{\mathrm{Max}}\,(\mathbf{c}_{\mathrm{S}}) = 0.185\ (\mathbf{c}_{\mathrm{S}})^{1/3}$, where q_{Max} is expressed in Å^{-1}. This scaling is valid for $\mathbf{c}_{\mathrm{S}} > 0.1$. Using for q_0 an average value taken from the data in Figure 11, *i.e.* $q_0 = 0.165 \pm 0.005$ Å^{-1}, we get for the surfactant concentration in the core $\mathbf{c}_{\mathrm{S}} \sim 0.70$! In terms of micellar volume fraction ϕ_{Mic} (assuming the density to be unity), this would mean that 70% of the volume of the core is occupied by surfactant micelles. This value is clearly too large. A reason for this discrepancy might be that the interaction potential between micelles in solution and in the dense core of the colloidal complexes are not the same, and so the structure factors might be slightly shifted with respect to each other [27].

There is another important result that can be used to estimate the micellar volume fraction ϕ_{Mic} in the core. It is related to the homopolyelectrolyte/surfactant system. Homopolyelectrolyte and surfactant in solutions undergo a phase separation, as previously described. If we consider specifically poly(sodium acrylate) and DTAB at concentration around 1%, the separation gives rise to a solid precipitate which displays the scattering features of a cubic phase of micelles. Identified by its sequence of Braggs reflections, the symmetry of the space group is $Pm3n$ [16], meaning 8 micelles per unit cell and a compacity of 0.524. Since the core of the colloidal complexes does not exhibit any crystallized structure, as said before, we conclude that the upper limit of the volume fraction of micelles in the

core must be less than 0.524. Note that we implicitly assume here that the mechanism of formation of the colloidal complexes is similar to the one driving the phase separation. We thus take $\phi_{\rm Mic} = 0.5$. The number of micelles per aggregates is then obtained using

$$N_{\rm Agg}^{\rm Mic} = \phi_{\rm Mic} \left(\frac{R_{\rm C}}{R_{\rm Mic}} \right)^3 .$$

Values for $N_{\rm Agg}^{\rm Mic}$ are given in Table 3 for the series at $\mathbf{c} = 1\%$ and, depending on Z, they range between 100 and 400.

For the determination of the number $N_{\rm Agg}^{\rm P}$ of diblock copolymers per aggregates, we use a result of Figure 5b that has not been discussed so far. The scattering intensity at $Z = 10$ reveals a specific feature in addition to the signature of the colloidal complexes (strong forward scattering and structure peak at q_0): at large wave vectors, the decrease of the intensity is reminiscent of that of pure DTAB/D_2O solution (also shown in Fig. 5b, $Z = \infty$). This scattering at $Z = 10$ can then be interpreted qualitatively as arising from two types of particles: the colloidal complexes and DTA micelles. This coexistence can also be guessed from the solution at $Z = 5$. With this observation, we emphasize that for solutions prepared with an excess of surfactants (large Z), all the PANa-PAM block copolymers are most likely incorporated into the complexes. Using then equation (3) to calculate the number density of colloids $n(Z)$, and assuming $\phi_{\rm Mic} = 0.5$ as previously determined, we get for the number of polymers per micelle in the aggregate a ratio of the order of 2/3. Thus, $N_{\rm Agg}^{\rm P} \sim (2/3) N_{\rm Agg}^{\rm Mic}$. With the values for $N_{\rm Agg}^{\rm Mic}$ as listed in Table 3, we obtained aggregation numbers $N_{\rm Agg}^{\rm P}$ varying from 70 to 250. These relatively low values are indicative of a corona which is not very dense. The density of chains starting from the core surface is estimated around 10^{-4} Å^{-2}.

4.2.4 Some arguments about the non-equilibrium nature of the colloidal complexes

The colloidal complexes evidenced so far have a microstructure very similar to that of polymeric micelles made from diblock copolymers in selective solvent [28]. Both exhibit core-shell organization, with respective sizes determined by the degree of polymerization of the blocks. The colloids produced by the association of polyelectrolyte/neutral diblocks and oppositely charged surfactants are however different from polymeric micelles. They do not result from a self-assembly mechanism, as surfactant or hydrophobic-hydrophilic diblocks do. As we show here, this class of aggregates depends on the preparation and mixing conditions. In Figure 14 are shown two scattering spectra labeled A and C (and three in the inset labeled A, B and C) obtained from solutions containing all 1% of polymers and surfactants in a ratio $Z = 1$. Their scattering features should thus be identical to that of the

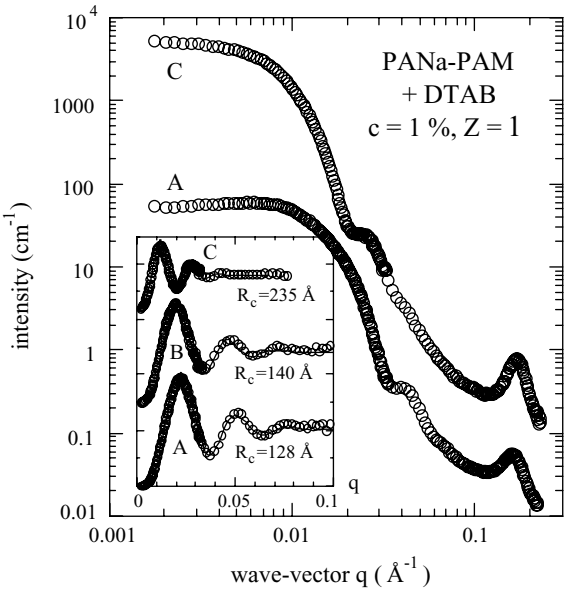

Fig. 14. Neutron scattering intensities obtained for three PANa-PAM/DTAB solutions (A, B and C), all containing the same amount of copolymers and surfactants, $\mathbf{c} = 1\%$ and $Z = 1$. A and C are shown as $I(q)$, whereas in the inset we used a Porod representation for the three samples ($q^4 \times I(q)$ *versus* q). As explained in the text, A, B and C were prepared according to different protocols. The intensity for C has been multiplied by 10 for the sake of clarity. The continuous lines in the inset result from best-fit calculations using a distribution of spherical particles of average radius $R_{\rm C}$ (also indicated). This result is a strong indication that the colloidal complexes are non-equilibrium structures.

PANa-PAM/DTAB solution displayed in Figure 5b. Solutions A (respectively, B and C) were prepared by mixing polymer stock solutions at $\mathbf{c}_{\rm P} = 2\%$ (respectively, 5% and 20%) with surfactant solutions at the same concentration, in a ratio such as $Z = 1$. These samples were then diluted from 2%, 5% and 20% to a final concentration of $\mathbf{c} = 1\%$ by addition of solvent. In Figure 14, the intensities scattered by solutions A and C cannot be superimposed, especially at low wave vectors. For the sake of clarity, C was multiplied by 10 with respect to the actual data. From the Porod analysis (inset), we obtained radii of the cores $R_{\rm C} = 128$ Å, 140 Å and 235 Å for solutions A, B and C, respectively. This again demonstrates that, although the same kind of aggregates forms by mixing polymer and surfactant solutions, their characteristic sizes depend on how these mixing were done. Note, finally, that the complexes of Figure 14 are very stable since, even after months, C does not evolve into A. We then conclude that the colloidal complexes made from charged/neutral diblock copolymers and oppositely charged surfactants are non-equilibrium structures.

5 Conclusion

In this work, we have shown that polyelectrolyte/neutral block copolymers and oppositely charged surfactants

associate in aqueous solutions to form colloidal complexes. Using dynamical light scattering and small-angle neutron scattering, two types of complexes have been identified in the water-rich region of the (surfactant/copolymer/water) phase diagram. For surfactant-polymer ratios Z smaller than a threshold noted $Z_{\rm C}$, we show clear evidences of single surfactant micelles decorated by diblock copolymers. Since the surfactant concentration is low, these dressed micelles are very few and coexist with unassociated diblocks. Above $Z_{\rm C}$, the colloidal complexes reveal a more original core-shell microstructure. The core is constituted of densely packed surfactant micelles, most likely connected between them by the polyelectrolyte blocks. The outer part of the colloid is a corona and it is made from the neutral chains. A semi-quantitative interpretation of the scattering data allows to determine the core and the corona dimensions, as well as the average aggregation numbers of micelles and polymers per particle. We found for the core and corona radii around 150 Å and 400 Å, respectively. The average numbers of micelles and diblocks per aggregate are comparable and of the order of some hundreds. For $Z \gg Z_{\rm C}$, *i.e.* for solutions rich in surfactant, the colloidal complexes have been found to coexist with single micelles. The present results suggest that the colloids result from a kinetic reaction between surfactant micelles and block copolymers, rather than from a mechanism of self-assembly. As shown in Figure 14, this kinetic reaction depends on the initial mixing conditions of the different components, solvent, polymers and surfactant. We propose that the driving mechanism for the complex formation is similar to that involved in the phase separation of homopolyelectrolyte/surfactant systems. In the case of the charged/neutral block copolymers, the presence of the neutral blocks prevents the macroscopic phase separation from occurring.

The authors are grateful to Eric Kaler, Didier Roux and Lennard Picullel for fruitful discussions. Mathias Destarac and his group from the Centre de Recherches d'Aubervilliers are acknowledged for providing us with the copolymers. This work is partially funded by the National Science Foundation, grant number PHY99-07949.

References

1. J.C.T. Kwak (Editor), *Polymer-Surfactant Systems*, Surfactant Science Series, Vol. **77** (Marcel Dekker, New York, 1998).
2. P. Haronska, T.A. Vilgis, R. Grottenmüller, M. Schmidt, Macromol. Theory Simul. **7**, 241 (1998); R.R. Netz, J.-F. Joanny, Macromolecules **32**, 9026 (1999); P. Welch, M. Muthukumar, Macromolecules **33**, 6159 (2000); F. Carlsson, P. Linse, M. Malmsten, J. Phys. Chem. B **105**, 9040 (2001).
3. K. Thalberg B. Lindman, K. Bergfeldt, Langmuir **7**, 2893 (1992).
4. A.J. Konop, R.H. Colby, Langmuir **15**, 58 (1999).
5. Y. Wang, K. Kimura, P.L. Dubin, W. Jaegger, Macromolecules **33**, 3324 (2000) and references therein.
6. M. Antonietti, J. Conrad, Angew. Chem., Int. Ed. **33**, 1869 (1994).
7. Y.V. Khandurina, A.T. Dembo, V.B. Rogacheva, A.B. Zezin, V.A. Kabanov, Polym. Sci. **36**, 189 (1994).
8. F. Yeh, L. Sokolov, A.R. Khokhlov, B. Chu, J. Am. Chem. Soc. **118**, 6615 (1996).
9. P. Ilekti, L. Piculell, F. Tournilhac, B. Cabanne, J. Phys. Chem. B **102**, 344 (1998); P. Ilekti, T. Martin, B. Cabanne, L. Piculell, J. Phys. Chem. B **103**, 9831 (1999).
10. E. Sokolov, F. Yeh, A. Khokhlov, V.Y. Grinberg, B. Chu, J. Phys. Chem. B **102**, 7091 (1998).
11. S. Zhou, B. Burger, F. Yeh, B. Chu, Macromolecules **31**, 8157 (1998).
12. A. Svensson, L. Piculell, B. Cabanne, P. Ilekti, J. Phys. Chem. B **106**, 1013 (2002).
13. H.S. Ashbaugh, B. Lindman, Macromolecules **34**, 1522 (2001).
14. K. Kogej, G. Evmenenko, E. Theunissen, H. Berghmans, H. Reynaers, Langmuir **17**, 3175 (2001).
15. S. Zhou, H. Hu, B. Burger, B. Chu, Macromolecules **34**, 1772 (2001).
16. J.M. Seddon, J. Robins, T. Gulick-Krywicki, H. Delacroix, Phys. Chem. Chem. Phys. **2**, 4485 (2000).
17. P. Hansson, Langmuir **17**, 4167 (2001).
18. T.K. Bronich, A.V. Kabanov, V.A. Kabanov, K. Yu, A. Eisenberg, Macromolecules **30**, 3519 (1997); T.K. Bronich, A.M. Popov, A. Eisenberg, V.A. Kabanov, A.V. Kabanov, Langmuir **16**, 481 (2000).
19. A.V. Kabanov, T.K. Bronich, V.A. Kabanov, K. Yu, A. Eisenberg, J. Am. Chem. Soc. **120**, 9941 (1998).
20. T.K. Bronich, A.M. Popov, A. Eisenberg, V.A. Kabanov, A.V. Kabanov, Langmuir **16**, 481 (2000).
21. P. Hervé, M. Destarac, J.-F. Berret, J. Lal, J. Oberdisse, I. Grillo, Europhys. Lett. **58**, 912 (2002).
22. D. Taton, A.-Z. Wilczewska, M. Destarac, Macromol. Rapid Commun. **22**, 1497 (2001).
23. B.L. Bales, R. Zana, J. Phys. Chem. B **106**, 1926 (2002).
24. Q. Ying, G. Wu, B. Chu, R. Farinato, L. Jackson, Macromolecules **29**, 4646 (1996).
25. B. Cabanne, R. Duplessix, T. Zemb, J. Phys. (Paris) **46**, 2161 (1985).
26. P.M. Claesson, M. Bergström, A. Dedinaite, M. Kjellin, J.-F. Legrand, I. Grillo, J. Phys. Chem. **104**, 11689 (2000).
27. R. Klein, B. D'Aguanno, in *Light Scattering Principles and Developments*, edited by W. Brown (Oxford University Press, Oxford, 1996) pp. 30-102.
28. A. Halperin, M. Tirrell, T.P. Lodge, Adv. Polym. Sci. **100**, 33 (1991); R. Nagarajan, K. Ganesh, J. Chem. Phys. **90**, 5843 (1989).